

Spreadsheet Fluid Dynamics for Aeronautical Course Problems*

ETSUO MORISHITA, YOHEI IWATA, KENTARO YUKI and HARUHIKO YOSHIDA
Graduate School of Engineering, Department of Aeronautics and Astronautics, University of Tokyo, 7-3-1,
Hongo, Bunkyo-ku, Tokyo, 113-8656, Japan. E-mail: morisita@fanno.t.u-tokyo.ac.jp

Computational Fluid Dynamics is now used daily in scientific and engineering practices. The computations themselves are now based on commercially available software. Personal computers are widely utilized elsewhere these days and many people are using spreadsheets as well as word processors. It is now well known to the scientific and engineering communities that spreadsheets can be used, not only for statistics and data processing calculations, but also for matrix inverse, iteration in a finite difference equation, and for special functions of mathematics. This situation allows us to realize SFD, i.e., Spreadsheet Fluid Dynamics. The authors have demonstrated that the fluid dynamics equations could be solved efficiently by using a spreadsheet. The cells in the spreadsheet are viewed as either natural grids in CFD or elements of a matrix. The computational domain corresponds to the real physical shape and/or the computational space by grid generation. The result can be visualized on the same spreadsheet with inherent graphics. The pre- and post-processors are all in one in SFD.

AUTHOR'S QUESTIONNAIRE

1. The paper describes software/hardware/simulation tools which are suitable for students of the following courses: Aerodynamics, Fluid Mechanics, Gas Dynamics, Heat and Mass Transfer.
2. The level involved is for undergraduates (third and fourth year) and masters degree students.
3. New material covered by this paper includes spreadsheet applications to general aerodynamic and/or fluid dynamic problems from conventional calculations to the NS finite difference solutions.
4. The material is presented by means of classroom demonstration and homework assignments; samples are obtained via the Internet.
5. The following texts accompany the presented material:
Misner, C. W. & Cooney, P. J., *Spreadsheet Physics*, Addison-Wesley, 1991.
Gottfried, B. S., *Spreadsheet Tools for Engineers*, McGraw-Hill, 1996.
Walkenbach, J., *Excel 97 Bible*, IDG Books, 1996.
Morishita, E., Spreadsheet fluid dynamics, *J. Aircraft*, **36**, 4, 1999, pp. 720–723.
Morishita, E., et al., AIAA Paper 2000-0804, *38th Aerospace Sciences*.
6. SFD is now being tested in the classroom (potential flow and gas dynamics). Findings to date:
 - almost free from computational literacy problems;

- concentration on the subjects themselves;
 - quick understanding and progress in the numerical procedure;
 - animation by graphics very useful.
7. People who are not specialized in the numerical method are also benefited from this technique. A lengthy program can be replaced by a very simple spreadsheet in some cases.

NOMENCLATURE

A	= coefficient matrix
b	= vector
C_d	= drag coefficient
C_l	= lift coefficient
C_m	= moment coefficient
C_p	= pressure coefficient
C_Q	= torque coefficient
C_T	= thrust coefficient
c	= chord
K	= transonic similarity parameter
L	= lift, length
l	= panel length
M	= Mach number
m_0	= lift slope
N	= numbers of blades
n	= rps
p	= pressure
R	= propeller radius, residual
r	= radius
s	= distance
u, v	= velocity component
V	= velocity vector
V	= flight velocity

* Accepted 20 August 2000.

V_i	= induced velocity
V_R	= relative velocity
x, y	= coordinate
z	= complex variable
α	= angle of attack
β	= blade pitch angle
ϕ	= potential, effective-pitch angle
Γ	= circulation
γ	= vortex strength, specific heat ratio
η	= efficiency
ρ	= density
σ	= solidity (= $Nc/(\pi R)$)
τ	= thickness ratio
ω	= angular velocity, relaxation factor
ξ, η	= transformed coordinate
ζ	= complex variable

suffixes

cal	= calculation
c.p.	= center of pressure
exp	= experiment
i	= induced
i, j	= i, j node
inf	= infinity
n	= n -th iteration
th	= theoretical value
0	= zero lift, leading edge
2-D	= two-dimensional
∞	= infinity

INTRODUCTION

THE SPREADSHEET is a very powerful engineering tool and it is used widely for scientific and engineering calculations [1–4]. One of the authors proposed using a spreadsheet for aerodynamics problems [4]. The emergence of computational fluid dynamics enables us to obtain detailed information on flow fields. Our experience in computing was that it took a very long time to learn computer languages and it was sometimes very hard to obtain proper results in a limited time. The spreadsheet, however, is rather easy to use and almost instantaneous numerical simulations are possible.

A Spreadsheet Fluid Dynamics (SFD) function is to solve aerodynamic and fluid dynamics problems by using a spreadsheet. There are typically three types of SFD:

Type I: conventional spreadsheet calculation, including the use of engineering functions.

Type II: matrix inverse and vector product.

Type III: iteration in a finite difference equation.

Type I calculation was used for a propeller calculation [5, 6] in this paper. This method can be used for complex potential calculations like a potential flow around a circular cylinder [7] and an airfoil. Conventional spreadsheet calculations can also handle the numerical integration of ordinary differential equations by the Runge-Kutta

method so that the self-similar boundary layer equation [8–10] is solved.

In Type II, matrix inversion by spreadsheet is a very powerful function for engineering applications. In aeronautical problems, the panel method [11, 12] involves the solution of linear simultaneous equations. The two-dimensional solution is obtained instantly by a spreadsheet. The choice of airfoil is also very easy. The numerical technique for a three-dimensional wing is also possible. The lifting line theory [12, 13] and the vortex lattice methods [14] both involve the matrix inverse and these types of problems are solved quite easily.

Type III seems to be the most important one in SFD. The iteration and the circular reference functions of spreadsheets [3] make it possible to solve finite difference equations. The cells in the spreadsheet are recognized as grids in CFD. The procedure used to solve the transonic small disturbance equation [15–18] is presented in detail in the present paper. The Laplace [4], the Euler [19–21], and the Navier-Stokes equations can be handled by SFD III. The classical method of characteristics [22–24] is also included in this category. Fluid dynamic instability [4, 25–29] is also one of the interesting subjects relating to SFD III.

SFD I – CONVENTIONAL CALCULATION

SFD Type I is when the conventional spreadsheet calculation is applied to aerodynamic and fluid dynamic problems. Here, we introduce the procedure used to calculate propeller characteristics.

The characteristics of a propeller can be predicted rather well by the classical momentum-blade element theory [5]. The aerodynamic performances at each radius are compiled to obtain its complete characteristics. Figure 1 shows the cross-sectional view of the propeller blade [5].

The sectional lift, defined as normal to the local flow direction is given by:

$$dL = \frac{1}{2} \rho V_R^2 C_l c dr \quad (1)$$

Therefore, the potential thrust component becomes:

$$dT = dL \cos(\phi + \alpha_i) = \frac{1}{2} \rho V_R^2 C_l c dr \cos(\phi + \alpha_i) \quad (2)$$

The momentum theory predicts the induced velocity in the far wake and has a value of $2V_i \cos(\phi + \alpha_i)$. The momentum change across the propeller must be equal to equation (2), i.e.

$$dT = 2\pi dr \rho [V + V_i \cos(\phi + \alpha_i)] \times 2V_i \cos(\phi + \alpha_i) \quad (3)$$

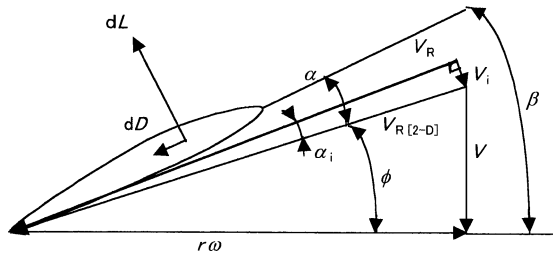


Fig. 1. Propeller section.

From equations (2) and (3), the induced angle of attack α_i in Fig. 1 is derived as follows [5]:

$$\alpha_i = \frac{\beta - \phi - \alpha_0}{1 + 8 \frac{r \sin \phi}{R \sigma m_0}} \quad (4)$$

Equation (4) is the first-order approximation and the more accurate second-order approximation is also obtainable. From equation (4), we obtain the sectional thrust dT and the torque dQ of the propeller as follows:

$$dT = N[dL \cos(\phi + \alpha_i) - dD \sin(\phi + \alpha_i)] \quad (5)$$

$$dQ = N[r dL \sin(\phi + \alpha_i) + r dD \cos(\phi + \alpha_i)] \quad (6)$$

Although we assume the potential flow to derive an induced angle of attack α_i , we include the viscous effect in equations (5) and (6). We can show that equations (5) and (6) become [5]:

$$\begin{aligned} \frac{dC_T}{dx} &= \frac{\pi^2 c N x^2 \cos^2 \alpha_i}{8R \cos^2 \phi} \\ \times (C_l \cos(\phi + \alpha_i) - C_d \sin(\phi + \alpha_i)) &\equiv \frac{\pi^3 \sigma x^2}{8} \lambda_T \end{aligned} \quad (7)$$

$$\begin{aligned} \frac{dC_Q}{dx} &= \frac{\pi^2 c N x^3 \cos^2 \alpha_i}{16R \cos^2 \phi} \\ \times (C_l \cos(\phi + \alpha_i) + C_d \sin(\phi + \alpha_i)) &\equiv \frac{\pi^3 \sigma x^3}{16} \lambda_Q \end{aligned} \quad (8)$$

Equations (7) and (8) can be numerically integrated (actually summed) by a spreadsheet.

The theory was compared to the experiment, R & M 829 No. 5 blade shape, a 4-blade wooden propeller [6]. We opened a spreadsheet and first specified the advance ratio V/nD as shown in cell C12 in Table 1. The value was chosen from Ref. 6 for the comparison. Six radial locations (row 14 in Table 1) were chosen after the R & M 829 [6]. The chord c , the zero-lift angle of attack α_0 and the number of blades N were obtained from Ref. 6 (rows 15-18 in Table 1). We calculated $\lambda \equiv V/(R\omega)$ in row 19 of Table 1. The solidity σ is calculated in row 20. The blade angles β were specified from Ref. 6 (rows 21 and 22 in Table 1).

Table 1. Propeller calculation (R&M829 4-blade wooden propeller [6])

	A	B	C	D	E	F	G	H
12	advance ratio	V/nD	1.0					
13								
14	radius/R	x (=r/R)	0.147	0.300	0.450	0.600	0.750	0.900
15	chord/R	c/R	0.128	0.135	0.163	0.164	0.145	0.102
16	0-lift angle of attack	α_0 [rad]	0.000	-0.105	-0.122	-0.096	-0.070	-0.052
17	0-lift angle of attack	α_0 [deg]	0.0	-6.0	-7.0	-5.5	-4.0	-3.0
18	number of blades	N	4	4	4	4	4	4
19	V/(R ω)	λ	0.318	0.318	0.318	0.318	0.318	0.318
20	Nc/(πR)	σ	0.163	0.172	0.207	0.209	0.185	0.129
21	blade angle	β [rad]	1.082	1.009	0.815	0.672	0.567	0.489
22	blade angle	β [deg]	62.0	57.8	46.7	38.5	32.5	28.0
23	effective-pitch angle	ϕ [rad]	1.137	0.815	0.616	0.488	0.401	0.340
24	effective-pitch angle	ϕ [deg]	65.2	46.7	35.3	27.9	23.0	19.5
25	lift slope ratio	$m_0/(2*\pi)$	1.0	1.0	1.0	1.0	1.0	1.0
26	induced angle of attack	α_i [rad]	-0.027	0.114	0.124	0.103	0.078	0.051
27	induced angle of attack	α_i [deg]	-1.544	6.535	7.092	5.914	4.470	2.914
28	lift coefficient	C_l	-0.176	1.159	1.243	1.112	0.991	0.944
29	drag coefficient	C_d	0.015	0.015	0.015	0.015	0.015	0.015
30	thrust component	λ_T	-0.520	1.430	1.342	1.180	1.023	0.973
31	torque component	λ_Q	-0.856	1.967	1.254	0.801	0.552	0.419
32	thrust derivative	dC_T/dx	-0.007	0.086	0.218	0.338	0.412	0.395
33	torque derivative	dC_Q/dx	-0.001	0.018	0.046	0.070	0.083	0.077
34								
35	thrust coefficient	C_T	0.216					
36	torque coefficient	C_Q	0.044					
37	efficiency	η	0.784					

The effective-pitch angle ϕ was calculated from:

$$\phi = \tan^{-1} \frac{V}{r\omega} = \tan^{-1} \frac{\lambda}{x} \quad (9)$$

For the cell C23, equation (9) was expressed: =ATAN(C19/C14). The two-dimensional airfoil characteristics were employed in the momentum-blade-element theory and the lift slope m_0 was assumed to be 2π in the present calculation (row 25 in Table 1). The induced angle of attack α_i was the obtained from equation (4) (rows 26 and 27 in Table 1). The sectional lift coefficient was then calculated as follows (row 28 in Table 1):

$$C_l = m_0(\beta - \phi - \alpha_0 - \alpha_i) \quad (10)$$

We assumed the sectional drag coefficient C_d to be 0.015 to take the viscous effect into account (row 29 in Table 1). We then calculated λ_T and λ_Q in equations (7) and (8) (rows 30 and 31 in Table 1). The thrust and torque radial gradients were also obtained from equations (7) and (8) (rows 32 and 33 in Table 1). The torque and thrust coefficients were calculated approximately by:

$$C_T = \sum \frac{dC_T}{dx} \Delta x \quad (11)$$

$$C_Q = \sum \frac{dC_Q}{dx} \Delta x \quad (12)$$

where $\Delta x = 0.15$ was employed for simplicity (C35 and C36 in Table 1). In C35, the spreadsheet command: =SUM(C32:H32)*0.15, was employed to calculate equations (11). Equation

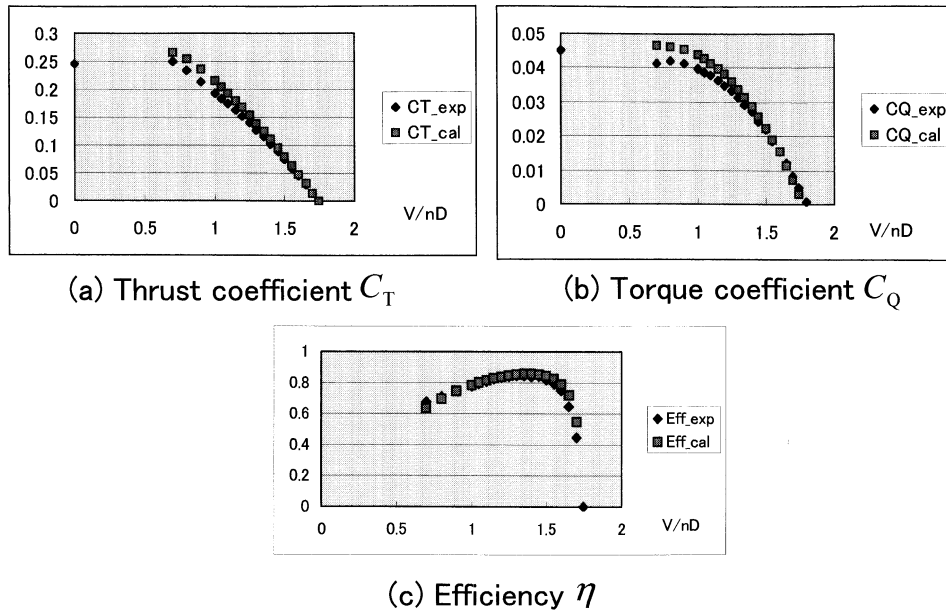


Fig. 2. Propeller characteristics (R&M829 4-blade wooden propeller [6]): (a) Thrust coefficient C_T ; (b) Torque coefficient C_Q ; (c) Efficiency η .

(12) was calculated similarly. The efficiency of the propeller was calculated by (C37 in Table 1):

$$\eta = \frac{C_T}{2\pi C_Q} \frac{V}{nD} \quad (13)$$

We repeated the calculation for each experimental advance ratio [6] to get a comparison and the results are shown in Fig. 2. Although a small difference is observed at a smaller advance ratio V/nD , the agreement is quite satisfactory in spite of the simplicity of the theory. The difference at the smaller advance ratio may be attributed to the constant sectional drag coefficient and the first-order approximation in the induced angle of attack. We recognize the negative thrust near the root for the given advance ratio in Table 1 and this happens at the off-peak efficiency operation. The variable-pitch propeller can minimize this type of loss and keep the optimum efficiency at a wide range of the advance ratio. The thrust and torque are both reduced at higher advance ratios because the average effective angle of attack is also reduced. When we further increase the advance ratio, we finally reach the point where neither thrust nor torque is produced.

SFD II – MATRIX INVERSE

One of the most convenient tools of spreadsheets is the function of matrix inverse, where a command ‘MINVERSE’ is employed [2]. The panel method [11, 12 pp. 260–288] is a typical example of SFD Type II.

The panel method is efficient for handling the lifting problem of a two-dimensional airfoil.

We use the vortex-based panel method and the potential is obtained for a flow around a two-dimensional airfoil as follows [11, 12]:

$$\phi(x, y) = U_\infty (x \cos \alpha + y \tan \alpha) + \sum_{j=1}^N \int_{\text{Panel } j} -\frac{\gamma(s)}{2\pi} \theta ds \quad (14)$$

where the linear vortex distribution [11, 12] is assumed along a panel in the present calculation, i.e.

$$\gamma(s) = \gamma_j + (\gamma_{j+1} - \gamma_j) \frac{s}{l_j} \quad (15)$$

$$\theta = \tan^{-1} \frac{y - y(s)}{x - x(s)} \quad (16)$$

We introduced the spreadsheet procedure to handle the panel method. First we specified the angle of attack as 10 degrees, and we converted it to radians as (H3 in Table 2(a)): =RADIANS(H2). We then specified the coordinate (x_j, y_j) of the j -th panel of the airfoil. The initial $j = 1-5$ is shown Table 2(b). A Karman-Trefftz airfoil [11] was used because the exact analytical solution was available. The transformation is given by:

$$\frac{\zeta - 1}{\zeta + 1} = \left(\frac{z - 1}{z + 1} \right)^k \quad (17)$$

The complex number represents a base circle that has a center at $z_0 = (-0.1, 0.1)$ and passes (1,0). $k = 1.7$ is in the present example. We employed 40 panels (i.e. 41 nodes) on the airfoil and the coordinates were actually obtained from the equally spaced points on the base circle. Care must

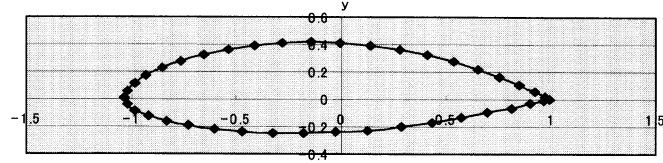


Fig. 3. Karman-Trefftz airfoil: $k = 1.7$, $z_0 = (-0.1, 0.1)$.

be taken at the trailing edge to avoid the singularity in the analytical solution by the complex potential method and we started from the point very close to the (1,0) on the circle. The spreadsheet commands, similar to: =IMREAL(G798), =IMAGINARY(G798), were used to obtain (x_j, y_j) . The nodes 1 and 41 were the trailing edge and the numbering of nodes was clockwise from the lower to the upper surface. The shape of the airfoil is readily available by selecting the graphics tool of the spreadsheet. We can use the chart wizard and select the XY(scatter)². In practice, the airfoil generation part was included in the same spreadsheet and the change of the airfoil was instantly possible by changing k and z_0 . The airfoil is shown in Fig. 3.

The length of the j th panel l_j and the coordinate of the midpoint of the same panel were then calculated (Table 2(b)):

$$l_j = \sqrt{(x_{j+1} - x_j)^2 + (y_{j+1} - y_j)^2} \quad (18)$$

$$x_{mj} = \frac{x_j + x_{j+1}}{2}, \quad y_{mj} = \frac{y_j + y_{j+1}}{2} \quad (19)$$

We introduced the local coordinate (x^*, y^*) of the panel j as shown in Fig. 4 [12].

The velocity potential due to the panel j is given by:

$$\phi(x^*, y^*) = -\frac{1}{2\pi} \int_l \left[\gamma_j + \frac{s}{l_j} (\gamma_{j+1} - \gamma_j) \right] \times \tan^{-1} \frac{y^*}{x^* - s} ds \quad (20)$$

The induced velocity by the panel j at the midpoint of the panel i is obtained from $\nabla\phi$ as follows:

$$u_{ij}^* = \frac{1}{2\pi} \left[\gamma_j + (\gamma_{j+1} - \gamma_j) \frac{x_{mi}^*}{l_j} \right] \beta_{ij} + \frac{1}{2\pi} (\gamma_{j+1} - \gamma_j) \frac{y_{mi}^*}{l_j} \ln \frac{r_{ij+1}^*}{r_{ij}^*} \quad (21)$$

$$v_{ij}^* = \frac{1}{2\pi} \left[\gamma_j + (\gamma_{j+1} - \gamma_j) \frac{x_{mi}^*}{l_j} \right] \ln \frac{r_{ij+1}^*}{r_{ij}^*} + \frac{1}{2\pi} (\gamma_{j+1} - \gamma_j) \left(1 - \frac{y_{mi}^*}{l_j} \beta_{ij} \right) \quad (22)$$

where

$$x_{mi}^* = (x_{mi} - x_j) \cos \theta_j + (y_{mi} - y_j) \sin \theta_j \quad (23)$$

$$y_{mi}^* = -(x_{mi} - x_j) \sin \theta_j + (y_{mi} - y_j) \cos \theta_j \quad (24)$$

$$r_{ij} = \sqrt{x_{mi}^{*2} + y_{mi}^{*2}} = \sqrt{\left(\frac{x_i + x_{i+1}}{2} - x_j \right)^2 + \left(\frac{y_i + y_{i+1}}{2} - y_j \right)^2} \quad (25)$$

$$\beta_{ij} = \tan^{-1} \frac{x_{mi}^*}{y_{mi}^*} + \tan^{-1} \frac{l_j - x_{mi}^*}{y_{mi}^*} \quad (i \neq j) \quad (26)$$

$$= \pi \quad (i = j)$$

The original coordinate system, and the induced velocities of equations (21) and (22) become:

$$u_{ij} = u_{ij}^* \cos \theta_j - v_{ij}^* \sin \theta_j \quad (27)$$

$$v_{ij} = u_{ij}^* \sin \theta_j + v_{ij}^* \cos \theta_j, \quad (28)$$

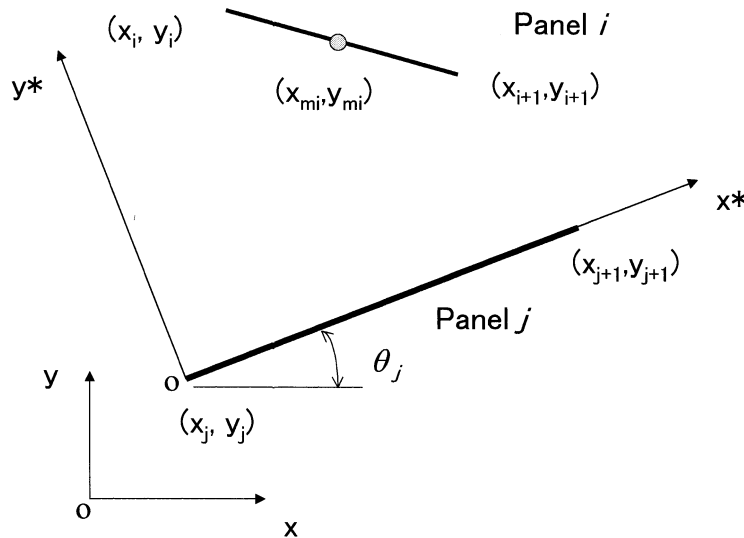


Fig. 4. Local coordinate of panel j .

Table 2(a). Angle of attack

	G	H
2	AOA [deg]	10
3	AOA [rad]	0.174532925

Table 2(b). Airfoil coordinates

	H	I	J	K	L	M
15	j	1	2	3	4	5
16						
17	x _j	1	0.9703	0.9044	0.8125	0.7005
18	y _j	0	-0.01	-0.032	-0.063	-0.098
19						
20	l _j	0.0314	0.0696	0.0968	0.1174	0.1329
21	x _{mid_j}	0.9851	0.9373	0.8585	0.7565	0.6366
22	y _{mid_j}	-0.005	-0.021	-0.048	-0.081	-0.116

Table 2(c). Calculation of r_{ij}

	F	G	H	I	J	K	L	M
83	r _{ij}							
84			x _j	1	0.9703	0.9044	0.8125	0.7005
85			y _j	0	-0.01	-0.032	-0.063	-0.098
86	x _{mid_i}	y _{mid_i}	i/j	1	2	3	4	5
87	0.9851	-0.005	1	0.0157	0.0157	0.0853	0.1821	0.2995
88	0.9373	-0.021	2	0.0662	0.0348	0.0348	0.1316	0.249
89	0.8585	-0.048	3	0.1494	0.118	0.0484	0.0484	0.1658
90	0.7565	-0.081	4	0.2565	0.2251	0.1555	0.0587	0.0587
91	0.6366	-0.116	5	0.3816	0.3503	0.2807	0.1839	0.0665

respectively. The velocity components at the midpoint of the panel i then become:

$$u_i(x_{mi}, y_{mi}) = U_\infty \cos \alpha + \sum_{j=1}^N u_{ij} \quad (29)$$

$$v_i(x_{mi}, y_{mi}) = U_\infty \sin \alpha + \sum_{j=1}^N v_{ij} \quad (30)$$

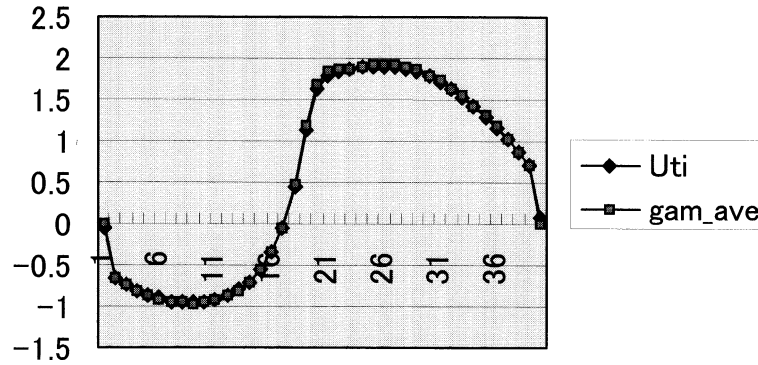
where U_{ni} the normal velocity component. Equation (31) is expressed as follows:

$$\begin{pmatrix} a_{11} & a_{12} & \dots & a_{1N} & a_{1N+1} \\ a_{21} & a_{22} & \dots & a_{2N} & a_{2N+1} \\ \dots & \dots & \dots & \dots & \dots \\ a_{N1} & a_{N2} & \dots & a_{NN} & a_{NN+1} \\ 1 & 0 & \dots & 0 & 1 \end{pmatrix} \begin{pmatrix} \gamma_1 \\ \gamma_2 \\ \dots \\ \gamma_N \\ \gamma_{N+1} \end{pmatrix}$$

The flow tangency condition at the midpoint of the panel i is given by:

$$U_{ni} = u_i \sin \theta_i - v_i \cos \theta_i = 0 \quad (1 \leq i \leq N) \quad (31)$$

$$= \begin{pmatrix} b_1 \\ b_2 \\ \dots \\ b_N \\ 0 \end{pmatrix} \quad (32)$$


 Fig. 5. Tangential velocity U_{ti} , $(\gamma_i + \gamma_{i+1})/2$.

where

$$a_{i1} = A_{i1}, a_{ij} = A_{ij} + B_{ij-1} (j = 2, 3, \dots, N),$$

$$a_{iN+1} = B_{iN}, b_i = U_\infty \sin(\alpha - \theta_i) \quad (33)$$

$$A_{ij} = C \cos(\theta_i - \theta_j) + D \sin(\theta_i - \theta_j),$$

$$B_{ij} = E \cos(\theta_i - \theta_j) + F \sin(\theta_i - \theta_j) \quad (34)$$

$$C = \frac{1}{2\pi} \left[- \left(1 - \frac{x_{mi}^*}{l_j} \right) \ln \frac{r_{ij+1}}{r_{ij}} + \left(1 - \frac{y_{mi}^*}{l_j} \beta_{ij} \right) \right],$$

$$D = \frac{1}{2\pi} \left[\left(1 - \frac{x_{mi}^*}{l_j} \right) \beta_{ij} - \frac{y_{mi}^*}{l_j} \ln \frac{r_{ij+1}}{r_{ij}} \right],$$

$$E = \frac{1}{2\pi} \left[- \frac{x_{mi}^*}{l_j} \ln \frac{r_{ij+1}}{r_{ij}} - \left(1 - \frac{y_{mi}^*}{l_j} \beta_{ij} \right) \right],$$

$$F = \frac{1}{2\pi} \left[\frac{x_{mi}^*}{l_j} \beta_{ij} + \frac{y_{mi}^*}{l_j} \ln \frac{r_{ij+1}}{r_{ij}} \right] \quad (35)$$

The last row of equation (32) represents the Kutta condition at the trailing edge, i.e.

$$\gamma_1 + \gamma_{N+1} = 0 \quad (36)$$

To solve the flow around an airfoil, it is necessary to construct the matrix in the LHS of equation (32) in the spreadsheet. The matrix was constructed step by step. To calculate r_{ij} in equation (25), we prepared 40×40 cells, a section of which is shown in Table 2(c).

In cell I87 we have equation (25) as follows:

$$=SQRT((I\$84-\$F87)^2+(I\$85-\$G87)^2).$$

We copied the equation onto the rest of the cells. When we refer to row 84, we use the \$ symbol [3], which is called the absolute reference, or otherwise the alphabet and the numbers are changed automatically corresponding to the location of the cells (relative reference [3]). We made 40×40 cells also for r_{ij+1} .

The midpoint of the panel i is obtained from equations (23) and (24) in the local coordinate of panel j . The upper left 5×5 cells out of the 40×40 cells for x_{mi}^* is shown in Table 2(d). Similar 40×40 cells were prepared for y_{mi}^* . We further proceeded to prepare several 40×40 cells in the same spreadsheet for $\ln(r_{ij+1}/r_{ij})$, β_{ij} , C , D , E , F , A_{ij} and B_{ij} based on equations (25), (26),

(34) and (35). We could finally prepare equation (32) with the 41×41 matrix based on equation (33) (Table 2(e)).

The most interesting part of this spreadsheet calculation is the solution procedure of equation (32). Equation (32) can be expressed symbolically as:

$$\mathbf{A}\boldsymbol{\gamma} = \mathbf{b} \quad (37)$$

and the solution is given by:

$$\boldsymbol{\gamma} = \mathbf{A}^{-1}\mathbf{b} \quad (38)$$

\mathbf{A}^{-1} in equation (38) is expressed in this calculation: =MINVERSE(I677:AW717). Then the solution $\boldsymbol{\gamma} = \mathbf{A}^{-1}\mathbf{b}$ is obtained as (column AY):

$$=MMULT(MINVERSE(I677:AW717), BA677:BA717).$$

To enter MINVERSE and/or MMULT command in the spreadsheet, we have to follow the particular key procedure for the software we use [2] (for example: input the equation in a cell, return key, select matrix and or vector area to input, set cursor at the end of the equation in the input area, then control + shift + return).

Once the vortex distribution is determined, the tangential velocity U_{ti} at the midpoint of the panel i is calculated from equations (27)–(30) as follows:

$$U_{ti} = u_i \cos \theta_i + v_i \sin \theta_i \quad (1 \leq i \leq N) \quad (39)$$

Another (and more efficient) approach [12] may be:

$$U_{ti} \cong \frac{\phi_{i+1} - \phi_i}{l_i} = \gamma_{im} = \frac{\gamma_i + \gamma_{i+1}}{2} \quad (1 \leq i \leq N) \quad (40)$$

Equations (39) and (40) are compared in Fig. 5, and give nearly the same value.

The pressure distribution is obtained from:

$$C_{pi} = 1 - \frac{U_{ti}^2}{U_\infty^2} \quad (1 \leq i \leq N) \quad (41)$$

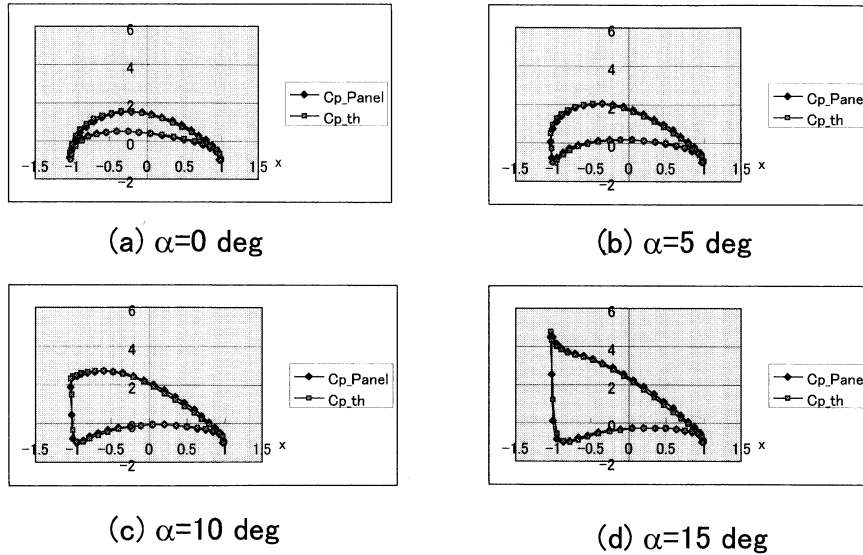


Fig. 6. $-C_p$ of Karman-Trefftz airfoil: $k = 1.7$, $z_0 = (-0.1, 0.1)$. (a) $\alpha = 0$ deg; (b) $\alpha = 5$ deg; (c) $\alpha = 10$ deg; (d) $\alpha = 15$ deg.

The aerodynamic characteristics are obtained from equation (41) as follows:

$$C_l = \sum_{i=1}^N (-C_{xi} \sin \alpha + C_{yi} \cos \alpha) \quad (42)$$

$$C_d = \sum_{i=1}^N (C_{xi} \cos \alpha + C_{yi} \sin \alpha) \quad (43)$$

$$C_{m0} = \sum_{i=1}^N \left(\frac{y_i + y_{i+1}}{2c} C_{xi} - \frac{x_i + x_{i+1}}{2c} C_{yi} \right) \quad (44)$$

$$\frac{x_{c.p.}}{c} = -\frac{C_{m0}}{C_l} \quad (45)$$

where

$$C_{xi} = \frac{y_{i+1} - y_i}{c} C_{pi}, \quad C_{yi} = -\frac{x_{i+1} - x_i}{c} C_{pi} \quad (46)$$

A simpler alternative method to calculate the lift coefficient is:

$$C_l = \frac{\rho U_\infty \Gamma}{\frac{1}{2} \rho U_\infty^2 c} = \frac{2\Gamma}{U_\infty c} = \frac{2 \sum_{i=1}^N \left(\frac{\gamma_i + \gamma_{i+1}}{2} \right) l_j}{U_\infty c} \quad (47)$$

Several solutions for this airfoil at different angles of attack are shown in Fig. 6. The lift coefficient $C_l = 2.1$ and the center of pressure 43% from the leading edge were obtained at $\alpha = 10$ degrees based on the approximate chord length $c \approx 2$. The angle of attack was changed in a cell of a spreadsheet and the solutions seen in Fig. 6 were obtained one after another while we were viewing the graph. (This can be done via a PC projector in the classroom and it is not surprising that students are impressed not only by the aerodynamics but also by the spreadsheets.)

The validity of the panel method was checked against the conformal mapping method of the

complex potential for the same airfoil (C_{p_th} in Fig. 6). The agreement is found to be quite satisfactory. (It has to be mentioned that the conformal mapping was also conducted on the same spreadsheet including the complex variable calculation.)

Care must be taken to avoid an airfoil with a very thin trailing edge which sometimes makes it difficult to obtain accurate solutions due to the interactions between singularities in the present panel method.

SFD III – ITERATION

Partial differential equations are solved numerically in discretized forms. Solutions are obtained via either relaxation or by a time-marching procedure. These require iterations during the process. SFD Type III handles these problems, i.e. most typically the numerical solution of finite difference equations [4]. The SFD technique was also extended to the more complicated transonic problems [15] by using the transonic small disturbance equation (TSDE) [12 (pp. 399–423) 16–18]:

$$\left[K - (\gamma + 1) M_\infty^2 \frac{\partial \phi}{\partial \xi} \right] \frac{\partial^2 \phi}{\partial \xi^2} + \frac{\partial \phi}{\partial \eta^2} = 0 \quad (48)$$

where

$$K = \frac{1 - M_\infty^2}{\tau^{2/3}}, \quad \xi = \frac{x}{c}, \quad \eta = \frac{y}{\Delta}, \quad (49)$$

$$\Delta = \frac{c}{\tau^{1/3}}, \quad \phi = \frac{\phi'}{U_\infty L}$$

where K is called the transonic similarity parameter, ϕ' represents the disturbance potential with dimensions. The airfoil is given by:

$$\frac{y(x)}{c} = \tau f\left(\frac{x}{c}\right) \quad (50)$$

and the non-dimensional flow tangency condition on the airfoil is:

$$\frac{\partial \phi}{\partial \eta} = \frac{df}{d\xi} - \frac{\alpha}{\tau} \quad (\eta = \pm 0) \quad (51)$$

The far-field boundary condition is given by:

$$\phi = 0 \quad (52)$$

The Murman-Cole method [12, 15–18] to solve equation (48) is:

$$(1 - \mu_{ij})P_{ij} + \mu_{i-1j}P_{i-1j} + Q_{ij} = 0 \quad (53)$$

where

$$\begin{aligned} P_{ij} &= \left[K - (\gamma + 1)M_\infty^2 \frac{\phi_{i+1j} - \phi_{i-1j}}{2\Delta\xi} \right] \\ &\quad \times \frac{\phi_{i+1j} - 2\phi_{ij} + \phi_{i-1j}}{\Delta\xi^2} \\ Q_{ij} &= \frac{\phi_{ij+1} - 2\phi_{ij} + \phi_{ij-1}}{\Delta\eta^2} \\ \mu_{ij} &= 1 \quad \text{for } A_{ij} < 0 \quad (M_{ij} > 1) \\ &= 0 \quad \text{for } A_{ij} \geq 0 \quad (M_{ij} \leq 1) \\ A_{ij} &= K - (\gamma + 1)M_\infty^2 \frac{\phi_{i+1j} - \phi_{i-1j}}{2\Delta\xi} \quad (54) \end{aligned}$$

Equation (53) implies that the upwind differencing is to be used at the supersonic point. The iterative solution may be obtained from:

$$\phi_{ij}^{(n+1)} = \phi_{ij}^{(n)} + C_{ij}^{(n)} \quad (55)$$

where we define:

$$C_{ij}^{(n)} \equiv \omega(\phi_{ij}^{(n+1)} - \phi_{ij}^{(n)}) \equiv \omega\delta\phi_{ij}^{(n)} \quad (56)$$

Note that $\phi_{ij}^{(n+1)}$ in equation (56) is a temporal value for the $n + 1$ iteration except for $\omega = 1$. We may have from equations (54):

$$\begin{aligned} P_{ij} &= \left[K - (\gamma + 1)M_\infty^2 \frac{\phi_{i+1j}^{(n)} - \phi_{i-1j}^{(n+1)}}{2\Delta\xi} \right] \\ &\quad \times \frac{\phi_{i+1j}^{(n)} - 2(\phi_{ij}^{(n)} + \delta\phi_{ij}^{(n)}) + \phi_{i-1j}^{(n+1)}}{\Delta\xi^2} \\ &= P_{ij}^{(n)} - \frac{2}{\Delta\xi^2} A_{ij}^{(n)} \delta\phi_{ij}^{(n)} \quad (57) \\ P_{i-1j} &= \left[K - (\gamma + 1)M_\infty^2 \frac{\phi_{ij}^{(n)} - \phi_{i-2j}^{(n+1)}}{2\Delta\xi} \right] \\ &\quad \times \frac{\phi_{ij}^{(n)} + \delta\phi_{ij}^{(n)} - 2\phi_{i-1j}^{(n+1)} + \phi_{i-2j}^{(n+1)}}{\Delta\xi^2} \\ &= P_{i-1j}^{(n)} + \frac{1}{\Delta\xi^2} A_{i-1j}^{(n)} \delta\phi_{ij}^{(n)} \quad (58) \end{aligned}$$

$$Q_{ij} =$$

$$\begin{aligned} &\frac{\phi_{ij+1}^{(n-1)} + \delta\phi_{ij+1}^{(n-1)} - 2(\phi_{ij}^{(n)} + \delta\phi_{ij}^{(n)}) + \phi_{ij-1}^{(n)} + \delta\phi_{ij-1}^{(n)}}{\Delta\eta^2} \\ &= Q_{ij}^{(n)} + \frac{\delta\phi_{ij+1}^{(n-1)} - 2\delta\phi_{ij}^{(n)} + \delta\phi_{ij-1}^{(n)}}{\Delta\eta^2} \quad (59) \end{aligned}$$

$P_{ij}^{(n)}$, $P_{i-1j}^{(n)}$, and $Q_{ij}^{(n)}$ are P_{ij} , P_{i-1j} , and Q_{ij} at $\delta\phi = 0$ in equations (57), (58) and (59), respectively. The updated values ($n+1$ th iteration) are also used in equations (57)–(59). Updated values are automatically used in real calculations. Here we use $\phi_{ij}^{(n)}$ in the bracket of equation (58) instead of $\phi_{ij}^{(n)} + \delta\phi_{ij}^{(n)}$ for simplicity and this assumption is different from Ref. 12. Similarly:

$$\begin{aligned} A_{ij}^{(n)} &= K - (\gamma + 1)M_\infty^2 \frac{\phi_{i+1j}^{(n)} - \phi_{i-1j}^{(n+1)}}{2\Delta\xi} \\ A_{i-1j}^{(n)} &= K - (\gamma + 1)M_\infty^2 \frac{\phi_{ij}^{(n)} - \phi_{i-2j}^{(n+1)}}{2\Delta\xi} \quad (60) \end{aligned}$$

$P_{ij}^{(n)}$, $P_{i-1j}^{(n)}$, and $Q_{ij}^{(n)}$ are expressed using equation (60):

$$P_{ij}^{(n)} = A_{ij}^{(n)} \frac{\phi_{i+1j}^{(n)} - 2\phi_{ij}^{(n)} + \phi_{i-1j}^{(n+1)}}{\Delta\xi^2} \quad (61)$$

$$P_{i-1j}^{(n)} = A_{i-1j}^{(n)} \frac{\phi_{ij}^{(n)} - 2\phi_{i-1j}^{(n)} + \phi_{i-2j}^{(n+1)}}{\Delta\xi^2} \quad (62)$$

$$Q_{ij}^{(n)} = \frac{\phi_{ij+1}^{(n-1)} - 2\phi_{ij}^{(n)} + Q_{ij-1}^{(n)}}{\Delta\eta^2} \quad (63)$$

Equation (53) uses equations (57)–(59) to obtain the following:

$$\begin{aligned} &-(1 - \mu_{ij}) \frac{2}{(\Delta\xi)^2} A_{ij}^{(n)} \delta\phi_{ij}^{(n)} \\ &+ \frac{\delta\phi_{ij+1}^{(n-1)} - 2\delta\phi_{ij}^{(n)} + \delta\phi_{ij-1}^{(n)}}{(\Delta\eta)^2} \\ &+ \mu_{i-1j} \frac{A_{i-1j}^{(n)}}{\Delta\xi^2} \delta\phi_{ij}^{(n)} = -R_{ij}^{(n)} \quad (64) \end{aligned}$$

where

$$R_{ij}^{(n)} = (1 - \mu_{ij})P_{ij}^{(n)} + \mu_{i-1j}P_{i-1j}^{(n)} + Q_{ij}^{(n)} \quad (65)$$

In the present calculation, we applied the relaxation factor ω for $\delta\phi_{ij}^{(n)}$ of equation (57), i.e. $\delta\phi_{ij}^{(n)}$ of the first term in the left-hand side of equation (64). We then obtained the following expression:

$$\begin{aligned} C_{ij}^{(n)} &= - \frac{1}{f\hat{\epsilon}\eta^2} (C_{ij-1}^{(n)} + C_{ij+1}^{(n-1)}) + R_{ij}^{(n)} \\ &\quad - 2(1 - f\hat{E}_{ij}) \frac{A_{ij}^{(n)}}{\omega\Delta\xi^2} + f\hat{E}_{i-1j} \frac{A_{i-1j}^{(n)}}{\Delta\xi^2} - \frac{2}{\Delta\eta^2} \quad (66) \end{aligned}$$

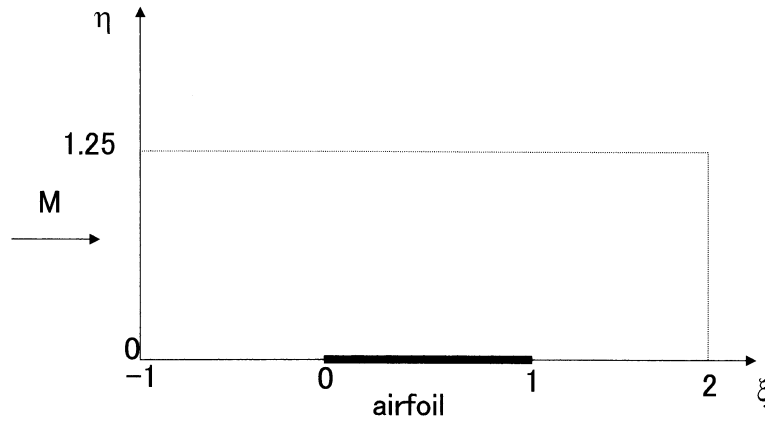


Fig. 7. Computational region.

Equation (66) is different from the solution technique in Ref. 12 (pp. 399–423). It is natural that one may assume the positive y-direction upwards in a spreadsheet. But the spreadsheet sweep is from left to right and from top to bottom, and therefore $C_{ij-1}^{(n)} + C_{ij+1}^{(n-1)}$ in equation (66) may become $C_{ij-1}^{(n-1)} + C_{ij+1}^{(n)}$ in the real calculation.

The basic computational domain is shown in Fig. 7 where $-1 \leq \xi \leq 2$, $0 \leq \eta \leq 1.25$ and the airfoil locates $0 \leq \xi \leq 1$, $\eta = 0$. $150(\xi) \times 25(\eta)$ cells with $\Delta\xi = 0.02$, $\Delta\eta = 0.05$ were used. The boundary cells were utilized in the latter part of the calculation, and 152×27 cells were used ultimately.

We are now able to start the spreadsheet calculation. The conditions for the calculation were first specified (rows 5 and 6 in Table 3(a)).

The specific heat ratio $\gamma = 1.4$ and the Mach number was 0.857. We used the iteration function of the spreadsheet and it is helpful in showing the number of iterations in cell L6. This

counter can be expressed by the spreadsheet format as: =L6+1.

This expression is called the circular reference in spreadsheet terminology [3] because cell L6 requires its own value, not given at the beginning. A warning message will appear on the screen, but we simply click the cancel button. When we start the iteration, 0 is resumed for cell L6 and therefore 1 will appear in cell L6 after one cycle.

Following the derivation of the transonic small disturbance equation (TSDE), we prepared the $150(\xi) \times 25(\eta)$ cells of $A_{ij}^{(n)}$ in equation (60) (Table 3(a)). In the cell D9, $A_{ij}^{(n)}$ is given by:

$$= \$I\$6 - (\$K\$6 + 1) / 2 /$$

$$\$B\$6 * (\$E\$6^2) * (E159 - C159)$$

and we copied the equation into the rest of the cells. The last bracket corresponds to the potential difference. The computational area in the spreadsheet corresponds to the physical space although a scaling factor exists and we know the subsonic

Table 3(a). Input conditions and $A_{ij}^{(n)}$

	A	B	C	D	E	F	G	H	I	J	K	L	M	N
1														
2		Transonic_small_disturbance_equation												
3														
4														
5		$\Delta\xi$	$\Delta\eta$	c	M	τ	Δ	ε	K	ω	γ	count		
6		0.02	0.05	1	0.857	0.06	2.554	0.153	1.733	0.9	1.4	21094		
7														
8		Aij	1.25											
9			1.2	1.733	1.684	1.684	1.684	1.684	1.683	1.683	1.682	1.681	1.681	1.681
10			1.15	1.733	1.685	1.685	1.684	1.684	1.684	1.683	1.683	1.682	1.681	1.681
11			1.1	1.733	1.686	1.686	1.686	1.685	1.685	1.685	1.684	1.683	1.683	1.682
12			1.05	1.733	1.688	1.688	1.688	1.688	1.687	1.687	1.686	1.686	1.685	1.684
13			1	1.733	1.691	1.691	1.691	1.691	1.69	1.69	1.689	1.689	1.688	1.687
14			0.95	1.733	1.695	1.695	1.695	1.694	1.694	1.694	1.693	1.692	1.692	1.691
15			0.9	1.733	1.7	1.7	1.7	1.699	1.699	1.698	1.698	1.697	1.696	1.695
16			0.85	1.733	1.706	1.705	1.705	1.705	1.704	1.704	1.703	1.703	1.702	1.701
17			0.8	1.733	1.712	1.712	1.712	1.711	1.711	1.711	1.71	1.709	1.709	1.708
18			0.75	1.733	1.72	1.719	1.719	1.719	1.719	1.718	1.718	1.717	1.716	1.715
19			0.7	1.733	1.728	1.728	1.728	1.727	1.727	1.727	1.726	1.725	1.724	1.724
20			0.65	1.733	1.737	1.737	1.737	1.737	1.736	1.736	1.735	1.735	1.734	1.733
21			0.6	1.733	1.747	1.747	1.747	1.747	1.747	1.746	1.746	1.745	1.744	1.744
22			0.55	1.733	1.758	1.758	1.758	1.758	1.758	1.757	1.757	1.756	1.756	1.755
23			0.5	1.733	1.77	1.77	1.769	1.769	1.769	1.769	1.769	1.768	1.768	1.767
24			0.45	1.733	1.782	1.782	1.781	1.781	1.781	1.781	1.781	1.781	1.781	1.78
25			0.4	1.733	1.794	1.794	1.794	1.794	1.794	1.794	1.794	1.794	1.794	1.794
26			0.35	1.733	1.806	1.806	1.806	1.806	1.806	1.806	1.806	1.807	1.807	1.807
27			0.3	1.733	1.817	1.818	1.818	1.818	1.818	1.819	1.819	1.819	1.82	1.821
28			0.25	1.733	1.828	1.828	1.829	1.829	1.83	1.83	1.831	1.832	1.832	1.833
29			0.2	1.733	1.838	1.838	1.839	1.839	1.84	1.84	1.841	1.842	1.844	1.845
30			0.15	1.733	1.846	1.846	1.847	1.847	1.848	1.849	1.85	1.852	1.853	1.855
31			0.1	1.733	1.852	1.853	1.853	1.854	1.855	1.856	1.857	1.859	1.86	1.862
32			0.05	1.733	1.856	1.856	1.857	1.858	1.859	1.86	1.861	1.863	1.865	1.867
33			0	1.733	1.857	1.858	1.858	1.859	1.86	1.861	1.863	1.865	1.867	1.869
34			-0.05											
35		η/ξ	-1.02	-1	-0.98	-0.96	-0.94	-0.92	-0.9	-0.88	-0.86	-0.84	-0.82	-0.8

Table 3(c). $C_{ij}^{(n)}$

	A	B	C	D	E	F	G	H	I	J	K	L	M	N
127														
128	C _{ij}	1.25		0	4E-08	8E-08	1E-07	2E-07	2E-07	3E-07	3E-07	3E-07	4E-07	4E-07
129		1.2		0	4E-08	8E-08	1E-07	2E-07	2E-07	3E-07	3E-07	3E-07	4E-07	4E-07
130		1.15		0	4E-08	8E-08	1E-07	2E-07	2E-07	3E-07	3E-07	3E-07	4E-07	4E-07
131		1.1		0	4E-08	8E-08	1E-07	2E-07	2E-07	3E-07	3E-07	3E-07	4E-07	4E-07
132		1.05		0	4E-08	8E-08	1E-07	2E-07	2E-07	3E-07	3E-07	3E-07	4E-07	4E-07
133		1		0	4E-08	8E-08	1E-07	2E-07	2E-07	3E-07	3E-07	3E-07	4E-07	4E-07
134		0.95		0	4E-08	8E-08	1E-07	2E-07	2E-07	3E-07	3E-07	3E-07	4E-07	4E-07
135		0.9		0	4E-08	8E-08	1E-07	2E-07	2E-07	3E-07	3E-07	3E-07	4E-07	4E-07
136		0.85		0	4E-08	8E-08	1E-07	2E-07	2E-07	3E-07	3E-07	3E-07	4E-07	4E-07
137		0.8		0	4E-08	8E-08	1E-07	2E-07	2E-07	3E-07	3E-07	3E-07	4E-07	4E-07
138		0.75		0	4E-08	8E-08	1E-07	2E-07	2E-07	3E-07	3E-07	3E-07	4E-07	4E-07
139		0.7		0	4E-08	8E-08	1E-07	2E-07	2E-07	3E-07	3E-07	3E-07	4E-07	4E-07
140		0.65		0	4E-08	8E-08	1E-07	2E-07	2E-07	3E-07	3E-07	3E-07	4E-07	4E-07
141		0.6		0	4E-08	8E-08	1E-07	2E-07	2E-07	3E-07	3E-07	3E-07	4E-07	4E-07
142	0.55		0	4E-08	8E-08	1E-07	2E-07	2E-07	3E-07	3E-07	3E-07	4E-07	4E-07	
143	0.5		0	4E-08	8E-08	1E-07	2E-07	2E-07	3E-07	3E-07	3E-07	4E-07	4E-07	
144	0.45		0	4E-08	8E-08	1E-07	2E-07	2E-07	3E-07	3E-07	3E-07	4E-07	4E-07	
145	0.4		0	4E-08	8E-08	1E-07	2E-07	2E-07	3E-07	3E-07	3E-07	4E-07	4E-07	
146	0.35		0	4E-08	8E-08	1E-07	2E-07	2E-07	3E-07	3E-07	3E-07	4E-07	4E-07	
147	0.3		0	4E-08	8E-08	1E-07	2E-07	2E-07	3E-07	3E-07	3E-07	4E-07	4E-07	
148	0.25		0	4E-08	8E-08	1E-07	2E-07	2E-07	3E-07	3E-07	3E-07	4E-07	4E-07	
149	0.2		0	4E-08	8E-08	1E-07	2E-07	2E-07	3E-07	3E-07	3E-07	4E-07	4E-07	
150	0.15		0	4E-08	7E-08	1E-07	1E-07	2E-07	2E-07	3E-07	3E-07	4E-07	4E-07	
151	0.1		0	3E-08	6E-08	1E-07	1E-07	2E-07	2E-07	2E-07	3E-07	3E-07	4E-07	
152	0.05		0	3E-08	6E-08	9E-08	1E-07	2E-07	2E-07	2E-07	3E-07	3E-07	4E-07	
153	0		0	3E-08	5E-08	8E-08	1E-07	1E-07	2E-07	2E-07	3E-07	3E-07	4E-07	
154														
155		η/ξ		-1	-0.98	-0.96	-0.94	-0.92	-0.9	-0.88	-0.86	-0.84	-0.82	-0.8

Table 3(d). Inlet ϕ_{ij}

	A	B	C	D	E	F	G	H	I	J	K	L	M	N	
157															
158	Φ _{ij}	1.25	-0	0	-0	-0	-0	-0	-0	-0	-0	-0	-0	-0	
159		1.2	-0	0	-0	-0	-0	-0	-0	-0	-0	-0	-0	-0	-0
160		1.15	-0	0	-0	-0	-0	-0	-0	-0	-0	-0	-0	-0	-0
161		1.1	-0	0	-0	-0	-0	-0	-0	-0	-0	-0	-0	-0	-0
162		1.05	-0	0	-0	-0	-0	-0	-0	-0	-0	-0	-0	-0	-0
163		1	-0	0	-0	-0	-0	-0	-0	-0	-0	-0	-0	-0	-0
164		0.95	-0	0	-0	-0	-0	-0	-0	-0	-0	-0	-0	-0	-0
165		0.9	-0	0	-0	-0	-0	-0	-0	-0	-0	-0	-0	-0	-0
166		0.85	-0	0	-0	-0	-0	-0	-0	-0	-0	-0	-0	-0	-0
167		0.8	-0	0	-0	-0	-0	-0	-0	-0	-0	-0	-0	-0	-0
168		0.75	-0	0	-0	-0	-0	-0	-0	-0	-0	-0	-0	-0	-0
169		0.7	-0	0	-0	-0	-0	-0	-0	-0	-0	-0	-0	-0	-0.01
170		0.65	-0	0	-0	-0	-0	-0	-0	-0	-0	-0	-0.01	-0.01	-0.01
171		0.6	-0	0	-0	-0	-0	-0	-0	-0	-0	-0.01	-0.01	-0.01	-0.01
172	0.55	-0	0	-0	-0	-0	-0	-0	-0	-0.01	-0.01	-0.01	-0.01	-0.01	
173	0.5	-0	0	-0	-0	-0	-0	-0	-0.01	-0.01	-0.01	-0.01	-0.01	-0.01	
174	0.45	-0	0	-0	-0	-0	-0	-0	-0.01	-0.01	-0.01	-0.01	-0.01	-0.01	
175	0.4	-0	0	-0	-0	-0	-0	-0.01	-0.01	-0.01	-0.01	-0.01	-0.01	-0.01	
176	0.35	-0	0	-0	-0	-0	-0	-0.01	-0.01	-0.01	-0.01	-0.01	-0.01	-0.01	
177	0.3	-0	0	-0	-0	-0	-0	-0.01	-0.01	-0.01	-0.01	-0.01	-0.01	-0.02	
178	0.25	-0	0	-0	-0	-0	-0.01	-0.01	-0.01	-0.01	-0.01	-0.01	-0.02	-0.02	
179	0.2	-0	0	-0	-0	-0	-0.01	-0.01	-0.01	-0.01	-0.01	-0.01	-0.02	-0.02	
180	0.15	-0	0	-0	-0	-0	-0.01	-0.01	-0.01	-0.01	-0.01	-0.02	-0.02	-0.02	
181	0.1	-0	0	-0	-0	-0	-0.01	-0.01	-0.01	-0.01	-0.01	-0.02	-0.02	-0.02	
182	0.05	-0	0	-0	-0	-0	-0.01	-0.01	-0.01	-0.01	-0.01	-0.02	-0.02	-0.02	
183	0	-0	0	-0	-0	-0	-0.01	-0.01	-0.01	-0.01	-0.01	-0.02	-0.02	-0.02	
184	-0.05	-0	0	-0	-0	-0	-0.01	-0.01	-0.01	-0.01	-0.01	-0.02	-0.02	-0.02	
185		η/ξ	-1.02	-1	-0.98	-0.96	-0.94	-0.92	-0.9	-0.88	-0.86	-0.84	-0.82	-0.8	
186															

158 = row 160 in Table 3(d). The symmetric boundary condition was applied along the ξ -axis ($\eta = 0$) and this means that row 184 = row 182 in Table 3(d) except on the airfoil surface ($0 \leq \xi \leq 1$).

The leading edge is cell BB183 and the airfoil is in row 183 in Table 3(e). The boundary condition equation (51) on the airfoil at $\alpha = 0$ is given by:

$$\frac{\phi_{i2} - \phi_{i0}}{2\Delta\eta} = \frac{df}{d\xi} \quad (0 \leq \xi \leq 1) \quad (67)$$

We used a parabolic airfoil in Fig. 8:

$$\frac{y}{c} = \tau f\left(\frac{x}{c}\right) = \tau 2 \frac{x}{c} \left(1 - \frac{x}{c}\right) \quad (68)$$

We obtain the following from equation (68):

$$\frac{df}{d\xi} = 2 - 4\xi \quad (69)$$

From equation (67), the boundary condition becomes:

$$\phi_{i0} = \phi_{i2} - 2\Delta\eta \frac{df}{d\xi} \quad (70)$$

Equation (70) for the cell BE184 in Table 3(e) is given by:

$$=BE182-2*\$C\$6*BE\$189.$$

Table 3(e). ϕ_{ij} on the airfoil

	A	B	AZ	BA	BB	BC	BD	BE	BF	BG	BH
157											
158	Φ_{ij}	1.25	0.015	0.016	0.017	0.018	0.019	0.02	0.021	0.022	0.024
159		1.2	0.015	0.016	0.017	0.018	0.019	0.02	0.021	0.023	0.024
160		1.15	0.015	0.016	0.017	0.018	0.019	0.02	0.021	0.022	0.024
161		1.1	0.014	0.015	0.016	0.017	0.019	0.02	0.021	0.022	0.023
162		1.05	0.014	0.015	0.016	0.017	0.018	0.019	0.02	0.021	0.023
163		1	0.013	0.014	0.015	0.016	0.017	0.018	0.019	0.02	0.022
164		0.95	0.011	0.012	0.013	0.014	0.015	0.017	0.018	0.019	0.02
165		0.9	0.009	0.01	0.011	0.013	0.014	0.015	0.016	0.018	0.019
166		0.85	0.007	0.008	0.009	0.01	0.012	0.013	0.014	0.016	0.017
167		0.8	0.004	0.005	0.007	0.008	0.009	0.01	0.012	0.013	0.015
168	0.75	0.001	0.002	0.003	0.004	0.006	0.007	0.009	0.01	0.012	
169	0.7	-0	-0	-0	6E-04	0.002	0.003	0.005	0.006	0.008	
170	0.65	-0.01	-0.01	-0.01	-0	-0	-0	3E-04	0.002	0.004	
171	0.6	-0.01	-0.01	-0.01	-0.01	-0.01	-0.01	-0.01	-0	-0	
172	0.55	-0.02	-0.02	-0.02	-0.02	-0.01	-0.01	-0.01	-0.01	-0.01	
173	0.5	-0.03	-0.03	-0.02	-0.02	-0.02	-0.02	-0.02	-0.02	-0.02	
174	0.45	-0.04	-0.03	-0.03	-0.03	-0.03	-0.03	-0.03	-0.03	-0.02	
175	0.4	-0.05	-0.04	-0.04	-0.04	-0.04	-0.04	-0.04	-0.04	-0.04	
176	0.35	-0.06	-0.06	-0.06	-0.06	-0.05	-0.05	-0.05	-0.05	-0.05	
177	0.3	-0.07	-0.07	-0.07	-0.07	-0.07	-0.07	-0.07	-0.07	-0.06	
178	0.25	-0.09	-0.09	-0.09	-0.09	-0.09	-0.09	-0.09	-0.09	-0.08	
179	0.2	-0.1	-0.11	-0.11	-0.11	-0.11	-0.11	-0.11	-0.11	-0.11	
180	0.15	-0.13	-0.13	-0.13	-0.13	-0.13	-0.14	-0.14	-0.14	-0.14	
181	0.1	-0.15	-0.15	-0.16	-0.16	-0.17	-0.17	-0.17	-0.17	-0.17	
182	0.05	-0.18	-0.19	-0.19	-0.2	-0.21	-0.21	-0.22	-0.22	-0.22	
183	0	-0.2	-0.22	-0.24	-0.26	-0.27	-0.28	-0.28	-0.28	-0.28	
184	-0.05	-0.18	-0.19	-0.39	-0.39	-0.39	-0.39	-0.39	-0.38	-0.37	
185	η/ξ	-0.04	-0.02	0	0.02	0.04	0.06	0.08	0.1	0.12	
186											
187		ξ			0	0.02	0.04	0.06	0.08	0.1	0.12
188		y/c			0	0.002	0.005	0.007	0.009	0.011	0.013
189		$df/d\xi$			2	1.92	1.84	1.78	1.68	1.6	1.52

Table 3(f). Outlet ϕ_{ij}

	A	B	ES	ET	EU	EV	EW	EX
157								
158	Φ_{ij}	1.25	0.117	0.117	0.117	0.117	0.117	0.117
159		1.2	0.117	0.117	0.117	0.117	0.117	0.117
160		1.15	0.117	0.117	0.117	0.117	0.117	0.117
161		1.1	0.117	0.118	0.118	0.118	0.118	0.118
162		1.05	0.118	0.118	0.118	0.118	0.118	0.118
163		1	0.119	0.12	0.12	0.12	0.12	0.12
164		0.95	0.121	0.121	0.121	0.121	0.121	0.121
165		0.9	0.123	0.123	0.123	0.123	0.123	0.123
166		0.85	0.125	0.125	0.125	0.125	0.125	0.125
167		0.8	0.127	0.127	0.127	0.127	0.127	0.127
168	0.75	0.13	0.13	0.13	0.13	0.13	0.13	
169	0.7	0.133	0.133	0.133	0.133	0.133	0.133	
170	0.65	0.136	0.136	0.136	0.136	0.136	0.136	
171	0.6	0.139	0.139	0.139	0.139	0.139	0.139	
172	0.55	0.142	0.142	0.142	0.142	0.142	0.142	
173	0.5	0.146	0.146	0.145	0.145	0.145	0.145	
174	0.45	0.149	0.149	0.149	0.149	0.149	0.149	
175	0.4	0.152	0.152	0.152	0.152	0.152	0.152	
176	0.35	0.156	0.155	0.155	0.155	0.155	0.155	
177	0.3	0.159	0.158	0.158	0.158	0.158	0.158	
178	0.25	0.161	0.161	0.161	0.161	0.161	0.161	
179	0.2	0.164	0.164	0.163	0.163	0.163	0.163	
180	0.15	0.166	0.165	0.165	0.165	0.165	0.165	
181	0.1	0.167	0.167	0.167	0.167	0.167	0.167	
182	0.05	0.168	0.168	0.168	0.168	0.167	0.168	
183	0	0.168	0.168	0.168	0.168	0.168	0.168	
184	-0.05	0.168	0.168	0.168	0.168	0.167	0.168	
185	η/ξ	1.9	1.92	1.94	1.96	1.98	2	

The outlet condition is given by:

$$\frac{d\phi}{d\xi} = 0 \tag{71}$$

In the finite difference form, equation (71) is given by:

$$\phi_{151j} = \phi_{149j} \tag{72}$$

In Table 3(f), this means column EX = column EV. The pressure coefficient is obtained as:

$$-C_{p_{ij}} = 2\tau^{2/3} \frac{\partial\phi}{\partial\xi} \Big|_{ij} \approx 2\epsilon \frac{\phi_{ij} - \phi_{i-1j}}{\Delta\xi} \tag{73}$$

We used equation (73) in the upwind difference from (Table 3(g)). The pressure distribution is shown in Fig. 9.

The present SFD result is compared to Ref. 18 for a 6% parabolic airfoil in Fig. 10. This is a supercritical case. The shock location was about the same, although an undesirable kink at the

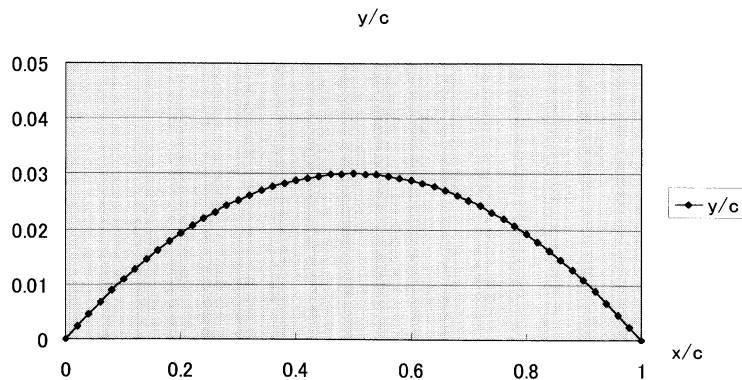


Fig. 8. Parabolic airfoil $\tau = 0.06$.

Table 3(g). Pressure coefficient $-C_{p_{ij}}$

	A	B	C	D	E	F	G	H	I	J	K	L	M	N
192		1.25		-0.01	0.008	0.008	0.008	0.008	0.008	0.009	0.009	0.009	0.009	0.009
193		1.2		-0.01	0.008	0.008	0.008	0.008	0.008	0.009	0.009	0.009	0.009	0.009
194	[-Cp ij]	1.15		-0.01	0.008	0.008	0.008	0.008	0.008	0.009	0.009	0.009	0.009	0.009
195		1.1		-0.01	0.008	0.008	0.008	0.008	0.008	0.008	0.008	0.008	0.009	0.009
196		1.05		-0.01	0.008	0.008	0.008	0.008	0.008	0.008	0.008	0.008	0.008	0.008
197		1		-0.01	0.007	0.007	0.007	0.007	0.007	0.007	0.007	0.008	0.008	0.008
198		0.95		-0.01	0.007	0.007	0.007	0.007	0.007	0.007	0.007	0.007	0.007	0.007
199		0.9		-0.01	0.006	0.006	0.006	0.006	0.006	0.006	0.006	0.006	0.006	0.006
200		0.85		-0	0.005	0.005	0.005	0.005	0.005	0.005	0.005	0.005	0.005	0.005
201		0.8		-0	0.004	0.004	0.004	0.004	0.004	0.004	0.004	0.004	0.004	0.004
202		0.75		-0	0.002	0.002	0.002	0.002	0.002	0.002	0.003	0.003	0.003	0.003
203		0.7		-0	8E-04	8E-04	8E-04	9E-04	9E-04	0.001	0.001	0.001	0.001	0.001
204		0.65		8E-04	-0	-0	-0	-0	-0	-0	-0	-0	-0	-0
205		0.6		0.003	-0	-0	-0	-0	-0	-0	-0	-0	-0	-0
206		0.55		0.004	-0	-0	-0	-0	-0	-0	-0	-0	-0	-0
207		0.5		0.006	-0.01	-0.01	-0.01	-0.01	-0.01	-0.01	-0.01	-0.01	-0.01	-0.01
208		0.45		0.009	-0.01	-0.01	-0.01	-0.01	-0.01	-0.01	-0.01	-0.01	-0.01	-0.01
209		0.4		0.011	-0.01	-0.01	-0.01	-0.01	-0.01	-0.01	-0.01	-0.01	-0.01	-0.01
210		0.35		0.013	-0.01	-0.01	-0.01	-0.01	-0.01	-0.01	-0.01	-0.01	-0.01	-0.01
211		0.3		0.015	-0.01	-0.01	-0.01	-0.01	-0.01	-0.01	-0.01	-0.02	-0.02	-0.02
212		0.25		0.017	-0.02	-0.02	-0.02	-0.02	-0.02	-0.02	-0.02	-0.02	-0.02	-0.02
213		0.2		0.018	-0.02	-0.02	-0.02	-0.02	-0.02	-0.02	-0.02	-0.02	-0.02	-0.02
214		0.15		0.02	-0.02	-0.02	-0.02	-0.02	-0.02	-0.02	-0.02	-0.02	-0.02	-0.02
215		0.1		0.021	-0.02	-0.02	-0.02	-0.02	-0.02	-0.02	-0.02	-0.02	-0.02	-0.02
216		0.05		0.021	-0.02	-0.02	-0.02	-0.02	-0.02	-0.02	-0.02	-0.02	-0.02	-0.02
217		0		0.022	-0.02	-0.02	-0.02	-0.02	-0.02	-0.02	-0.02	-0.02	-0.02	-0.02
218		-0.05		0.021	-0.02	-0.02	-0.02	-0.02	-0.02	-0.02	-0.02	-0.02	-0.02	-0.02
219		η/ξ		-1	-0.98	-0.96	-0.94	-0.92	-0.9	-0.88	-0.86	-0.84	-0.82	-0.8

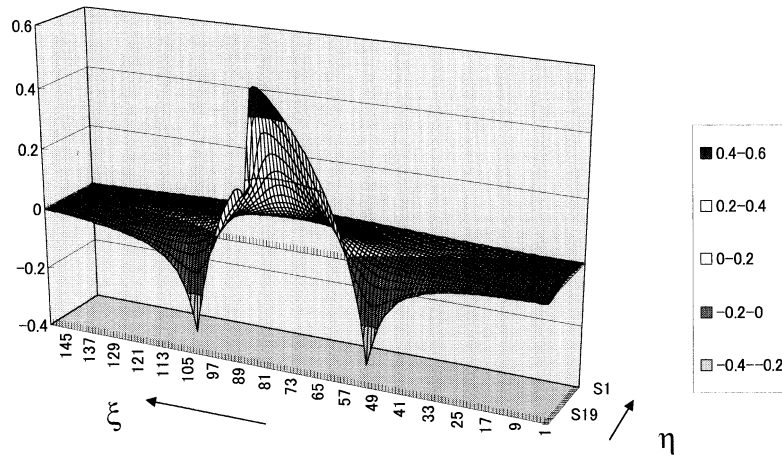


Fig. 9. Pressure distribution $-C_p$ at $M_\infty = 0.857$.

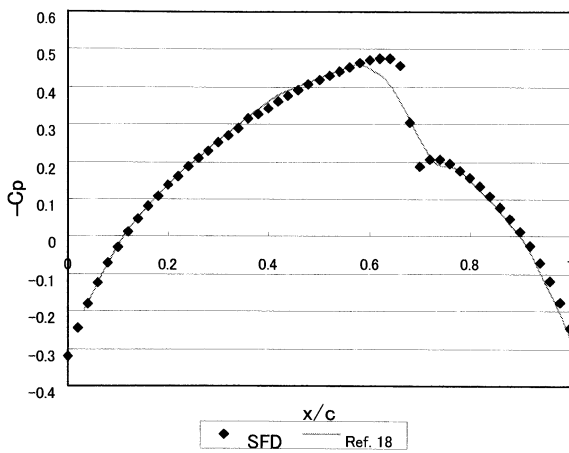


Fig. 10. Comparison of pressure distribution $-C_p$. Supercritical $M_\infty = 0.857$.

end of the shock was observed by the present technique. The sonic condition is given by $-C_p^* = 0.286$ at $M_\infty = 0.857$. It became supersonic around $x/c \approx 0.34 - 0.68$. The solution as a whole seems to be satisfactory in the present calculation, except around the shock wave. The present method was also applied for subcritical and lifting cases [15].

SFD FEATURES AND DISCUSSION

CFD problems have been historically solved by computer languages like Fortran and C. SFD can basically handle the same problems as CFD. In the learning stage of the numerical methods, the lack of computational literacy leads students and engineers to a laborious obstruction. Immature understanding of the subject makes the situation more difficult to carry out. SFD may be useful to the beginners at this stage. The cells correspond to

the physical and/or the computational space and the users easily identify the computational region and the boundary, i.e. it is relatively easy to realize where we are working. The cells of a spreadsheet do not accept the wrong format and we can be very sure about the formula. The division by zero, for example, is visible, and we can continue the calculation after corrections are made. The graphics are useful while we are checking the values during the calculation and the final results. The figures are still active after the calculation and the effect of parameters like the Reynolds and the Prandtl numbers can be shown quite easily simply by changing the values. It must be noted that a spreadsheet has Internet capability and it is even active on a web page. Therefore, we can provide our spreadsheet calculation via the Internet.

It is necessary to mention the drawbacks of SFD. It was often experienced that the computational region could not easily be changed after the spreadsheet was completed. Once we created a 20×20 cell spreadsheet, it was rather troublesome to increase it up to a 200×200 cell spreadsheet. In programming language, this can be achieved relatively easily. So the initial design is important in SFD. But if the spreadsheet can incorporate programming languages like Visual Basic [3], there might be a better way. It is often believed the computational speed is slower in SFD than that in CFD. This is true but the speed can be faster if we do not show the numbers in the cell. One of our colleagues once solved a three-dimensional heat conduction problem in the industry by SFD together with the Fortran coding. The Fortran program was faster in the computation itself, but SFD was actually more efficient when pre- and post-processing were included. This was because the results in the spreadsheet could be visualized almost instantly. In the present calculation, the solution was instantaneous for the propeller and the panel method. The transonic small disturbance calculation took less than an hour for around 20000 iterations by a conventional 400 MHz PC. The correction was $C_{ij}^{(n)} < 2 \times 10^{-6}$ after the iterations and the pressure C_p effectively did not change when we doubled the iterations.

The advanced software, such as Mathematica and MATLAB, which were sometimes used with SFD in a cooperative manner. The ordinary differential equation can be solved quite efficiently by Mathematica. We also solved the same equation by using a spreadsheet because the results are still active after doing the calculations and we can

check the effect of the divisions and boundary and/or initial conditions while we are viewing the active graphics. The visual solution development in time and iteration in SFD is very useful. On the other hand the velocity vector, for example, cannot be handled on a spreadsheet but we can utilize the MATLAB function in this case using the data from the spreadsheet. The advanced graphics and the large-scale matrix inverse are not readily available in the spreadsheet.

CONCLUDING REMARKS

In the present paper, conventional spreadsheet calculation was used to estimate propeller characteristics. Furthermore, the spreadsheet handles complex variables, engineering functions and so forth. This enables us to solve complex potential problems and other analytical aerodynamic problems with ease (SFD Type I).

The panel method was solved by the spreadsheet. The matrix inverse is incorporated in spreadsheets, and therefore the Prandtl's lifting line theory and the vortex lattice method can be solved easily. We prepared a matrix of the problem and a spreadsheet command, such as MINVERSE made an instantaneous solution from the equation (SFD Type II).

The most important aspect of SFD is the iterated solution of the finite difference equations of CFD. We have shown the results for the transonic small disturbance equation. The upwind difference was handled effectively by the spreadsheet command. The Laplace, Euler and Navier-Stokes equations are also solvable by this method. The computational domain for spreadsheets is rectangular, but this does not necessarily limit our computation to the Cartesian coordinate. The standard grid generation procedure is also used in SFD (SFD Type III).

In conclusion, SFD can solve most of the important aeronautical course problems (as well as the practical ones). The most important aspect of SFD is that less computer literacy is required for the user. This is particularly valuable to students and beginners using numerical simulations, as well as for engineers in the industry. We can mainly concentrate on fluid dynamic problems rather than programming problems when utilizing SFD. SFD can be used cooperatively with programming languages and other symbolic programming software.

REFERENCES

1. C. Misner and P. Cooney, Two-dimensional motion, *Spreadsheet Physics*, Addison-Wesley, Reading (1991) pp. 43–56.
2. B. S. Gottfried, Solving simultaneous equations, *Spreadsheet Tools for Engineers*, McGraw-Hill, New York (1996) pp. 179–212.

3. J. Walkenbach, Creating and using formulas, *Excel 97 Bible*, IDG Books Worldwide, Foster City (1996).
4. E. Morishita, Spreadsheet fluid dynamics, *J. Aircraft*, **36**, 41 (1999) pp. 720–723.
5. D. O. Dommasch, S. S. Sherby and T. F. Conolly, Vortex theory, *Airplane Aerodynamics*, Pitman, New York, 9 (1951) pp. 184–195.
6. A. Fage, C. N. H. Lock, R. G. Howard and H. Bateman, Experiments with a family of airscrews including the effect of tractor and pusher bodies, *Reports and Memoranda*, No. 829 (1922) p. 61.
7. I. Imai, A circular cylinder in arbitrary motion, *Fluid Dynamics* (in Japanese), Iwanami, Tokyo (1970) pp. 73–78.
8. S. Schreier, The Howarth Transformation, *Compressible Flow*, John Wiley & Sons, New York (1982) pp. 309–315.
9. E. R. van Driest, Turbulent boundary layer in compressible fluids, *J. Aeronautical Sciences*, **18**, 3 (1951) pp. 145–160.
10. F. W. Matting, D. R. Chapman, J. R. Nyholm and A. G. Thomas, Turbulent skin friction at high mach numbers and Reynolds numbers in air and helium, *NASA TR R-82* (1961) pp. 28–29.
11. A. Mizuno, Karman-Trefftz, wing section, *An Introduction to CFD* (in Japanese), Asakura, Tokyo (1990) pp. 80–96.
12. J. Moran, Nonelliptic Lift distributions, *An Introduction to Theoretical and Computational Aerodynamics*, John Wiley & Sons, New York (1984) pp. 124–153.
13. T. Moriya, Theory of Propeller, *An Introduction to Aerodynamics* (in Japanese), Baifukan, Tokyo (1970) pp. 177–200.
14. K. Yuki, Performance prediction of a two-blade propeller by vortex lattice method (in Japanese), graduation thesis, Department of Aeronautics and Astronautics, University of Tokyo (1999).
15. Y. Iwata, Flow around a two-dimensional airfoil solved by transonic small disturbance equation (in Japanese), graduation thesis, Department of Aeronautics and Astronautics, University of Tokyo (1999).
16. E. M. Murman, Analysis of embedded shock waves calculated by relaxation methods, *AIAA Journal*, **12**, 6 (1974) pp. 626–633.
17. E. D. Knechtel, Experimental investigation at transonic speeds of pressure distribution over wedge and circular arc sections and evaluation of perforated wall interference, *NASA TN D15* (1959).
18. D. J. Collins and J. A. Krupp, Experimental and theoretical investigations in two-dimensional transonic flow, *AIAA Journal*, **12**, 6 (1974) pp. 771–778.
19. H. Yoshida, Flow around a cavity solved by small disturbance and Euler equations (in Japanese), graduation thesis, Department of Aeronautics and Astronautics, University of Tokyo (1999).
20. K. Fujii, TVD scheme, *Numerical Methods for Computational Fluid Dynamics* (in Japanese), University of Tokyo Press (1994) pp. 68–76.
21. K. A. Hoffmann and S. T. Chiang, MacCormack explicit formulation, *Computational Fluid Dynamics for Engineers, II*, Engineering Education System, Wichita (1993) pp. 205–207.
22. C. Y. Chow, Propagation of a finite-amplitude wave: formation of a shock, *An Introduction to Computational Fluid Mechanics*, John Wiley & Sons, New York (1979) pp. 203–214.
23. J. D. Anderson, Jr., Determination of the compatibility equations, *Modern Compressible Flow with Historical Perspective*, McGraw-Hill, New York (1982) pp. 260–305.
24. A. H. Shapiro, Sharp-corner nozzle, *The Dynamics and Thermodynamics of Compressible Fluid Flow*, Vol. I, Ronald Press, New York (1953) pp. 512–516.
25. J. T. Stuart, On the non-linear mechanics of hydrodynamic stability, *J. Fluid Mechanics*, **4** (1958) p. 15.
26. Schlichting, Flow between concentric rotating cylinders, H, *Boundary-Layer Theory*, McGraw-Hill, New York (1979) pp. 525–529.
27. J. E. Burkhalter and E. L. Koschmieder, Steady supercritical Taylor vortices after sudden starts, *The Physics of Fluids*, **17**, 11 (1974) pp. 1929–1935.
28. M. van Dyke, 127, Axisymmetric laminar Taylor vortices, *An Album of Fluid Motion*, Parabolic Press, Stanford, 1982, pp. 76–77.
29. G. I. Taylor, Fluid friction between rotating cylinders I-torque measurements, *Proc. Royal Soc. London, Series A*, **157**, 1936 pp. 546–564.

Etsuo Morishita, Professor, Department of Aeronautics and Astronautics, Graduate School of Engineering, University of Tokyo. Japan, B.Eng. (1972), M. Eng. (1974), Dr.Eng. (1985), University of Tokyo, M.Sc. (1982), University of Cambridge, 1974–1987: Mitsubishi Electric Corporation, 1987–Present: University of Tokyo, Associate Professor (1987–1993), Professor (1993–). Achievements include scroll compressor and co-rotating scroll vacuum pump development at MELCO. Contributor to technical journals and international patents holder. Presently engaged in the education and the research of aerodynamics at the University of Tokyo. Name appeared in Who's Who in Science and Engineering 1994/1995(USA)

Yohei Iwata, graduate student (Master course 2nd year), Department of Aeronautics and Astronautics, Graduate School of Engineering, University of Tokyo. His current subject is 'Spreadsheet Fluid Dynamics of Unsteady Flows'. He solved the transonic small disturbance equation by SFD.

Kentaro Yuki, Presently Japanese Patent Office. Former graduate student (Master course), Department of Aeronautics and Astronautics, Graduate School of Engineering, University of Tokyo. He solved the propeller VLM by SFD.

Haruhiko Yoshida, graduate student (Master course 2nd year), Department of Aeronautics and Astronautics, Graduate School of Engineering, University of Tokyo. His current subject is 'A New Scheme for High-Speed Flows Based on the Time-Space Conservation'. He solved the Euler equation by SFD.